Transient behaviors of surface plasmon coupling with a light emitter

Wen-Hung Chuang, Jyh-Yang Wang, C. C. Yang,[a] and Yean-Woei Kiang[b]
Institute of Photonics and Optoelectronics and Department of Electrical Engineering, National Taiwan University, 1, Roosevelt Road, Section 4, Taipei 10617, Taiwan

(Received 23 July 2008; accepted 20 September 2008; published online 13 October 2008)

The transient behaviors of dipole couplings with surface plasmons (SPs) on a metal/dielectric grating interface, including surface plasmon polariton (SPP) and localized surface plasmon (LSP), are numerically demonstrated. Such a dipole-SP coupling process can lead to either enhanced dipole emission or effective pumping of a cavity-confining SP mode. Based on the time-resolved responses of a source pulse, it is found that the dipole-SP coupling features can be excited in several femtoseconds with the decay times ranging from 5 to 20 fs. From the significantly different decay times between the LSP and grating-assisted SPP features, one can classify those SP-coupling features into different application categories of efficient emission and SP energy storage. © *2008 American Institute of Physics*. [DOI: 10.1063/1.2998617]

The coupling of a radiation dipole with a surface plasmon (SP) generated on a nearby metal surface can lead to effective energy transfer from the dipole into the SP. This may have the application of emission enhancement or effective SP energy pumping.[1–9] The emission enhancement mechanism of SP coupling is useful for improving the efficiency of a light-emitting device. On the other hand, effective SP energy pumping is a crucial factor for implementing a system of SP amplification by stimulated emission of radiation (SPASER) besides the requirement of an effective SP-confining cavity.[10,11] The SP coupling with a radiation dipole is an effective approach for pumping SP energy. In either application, a metal grating of an appropriate period with properly designed groove geometry has been considered for use in supporting SPs.[6,7,12–15] The grating period is designed to match the momentum between surface plasmon polariton (SPP) and photon for effective coupling and/or emission. The design of the metal groove geometry aims at the generation of localized surface plasmons (LSPs) for effective coupling and/or emission. Also, a metal grating of appropriate geometry can be a good choice for forming an effective SP-confining cavity in the effort of implementing a SPASER system.[16] Although the SPP coupling in a metal grating structure has been widely discussed, the effect of LSP coupling in a similar structure was rarely studied. Also, although SP couplings with a quantum well or a dipole have been widely studied, they are limited to the frequency response. Transient behaviors of such a coupling process have not been reported yet. Such a study can help in elucidating the effectiveness of SP energy storage in an SP-dipole coupling system. It is useful for designing a metal nanostructure for either emission enhancement or SPASER implementation.

In this letter, we report the numerical simulation results on the transient behaviors of such a SP-dipole coupling process. The time-response functions at a few near-field locations of a pulsed radiation dipole located near a metal grating interface are evaluated. To simulate the transient field responses, we first calculate the electromagnetic field distribution in the frequency domain based on the boundary integral-equation method (BIEM)[17] and then take the inverse Fourier transform to obtain the time-resolved response.

The metal grating structure under study is shown in the insert of Fig. 1. Here, a periodical corrugation structure with a period $a=100$ nm and the single-groove shape governed by $y=-h\exp(-|x/d|^m)$ with $h=10$ nm, $m=6.73$, and $d=23.75$ nm are used. The grating interface separates a half space of Ag and a half space of dielectric. For numerical computation, the permittivity of Ag is assumed to follow the Drude model[18] with the angular plasma frequency set at $\omega_p=1.19\times10^{16}$ (rad s^{-1}) and damping constant set at $\gamma=1.33\times10^{14}$ (rad s^{-1}), leading to the SPP resonance energy at ~430 nm on a flat Ag/dielectric interface with the refractive index of the dielectric fixed at 2.5. A radiation dipole oriented along the x axis and labeled as J_x is placed at a position of 10 nm below a grating valley at $x=0$. The dipole and the grating structure are assumed to be infinitely extended along the $+z$ and $-z$ directions for defining a two-dimensional

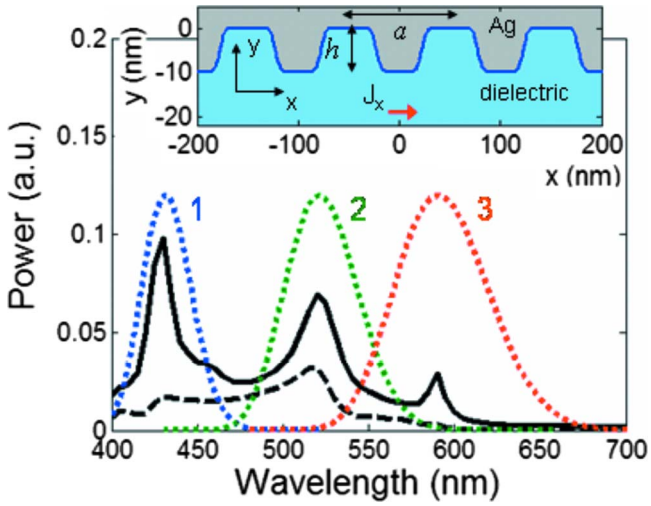

FIG. 1. (Color online) Dipole radiation power spectrum (continuous curve), the emission spectrum of the SP-dipole coupling system (dashed curve), and the three source spectra (dotted Gaussian-like curves labeled as 1–3). The insert shows the two-dimensional Ag/dielectric grating structure in the x-y plane. The dipole J_x is located 10 nm right below the center of a grating groove.

[a]Electronic mail: ccy@cc.ee.ntu.edu.tw.
[b]Electronic mail: ywkiang@ntu.edu.tw.

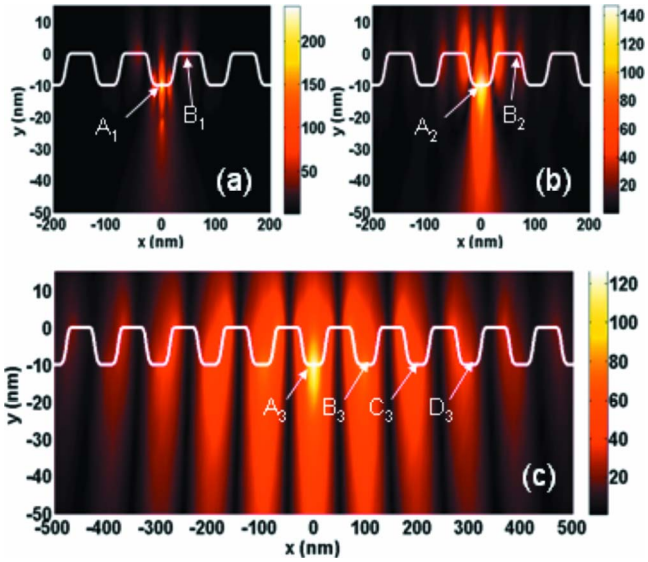

FIG. 2. (Color online) Single-frequency field magnitude distributions of features 1–3 in parts [(a)–(c)], respectively. The labeled positions are considered for transient study.

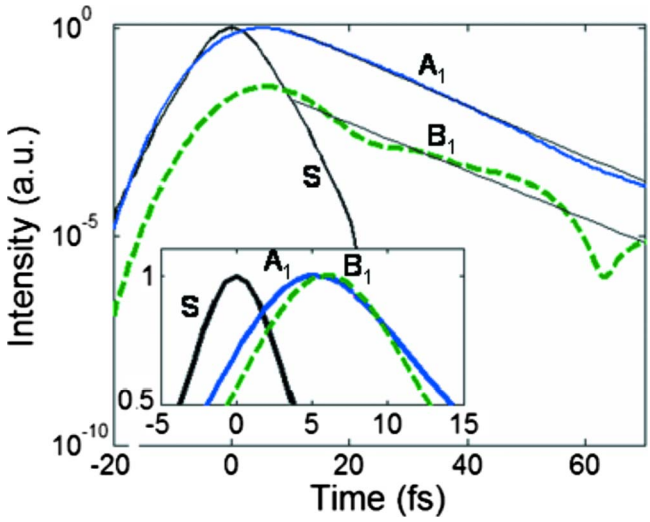

FIG. 3. (Color online) Time-resolved field intensity profiles at various observation points for feature 1. The inset at the bottom shows the linear-scale profiles for demonstrating the temporal peak positions.

problem. The two-dimensional problem geometry is reasonable for our study as we are mainly concerned with the grating-assisted SPP along the x axis and the z-invariable LSP features.

The continuous and dashed curves in Fig. 1 show the radiation power spectra of the dipole and the coupling-system emission, respectively. The dipole radiation power is obtained by integrating the outgoing Poynting vectors from a square boundary of 2.5 nm in dimension with the dipole at the center. It represents the dipole output under the SP-coupling condition. The system emission power is obtained by integrating the Poynting vectors in the $-y$ direction along a horizontal line 1 μm (far field) below the dipole. The system emission power is lower than the dipole radiation power due to the energy loss of metal dissipation and the SPP propagation along the $\pm x$ directions. The three major dipole radiation features in Fig. 1 are labeled as 1–3. Three source spectra of the same frequency distribution are defined for the three SP features, as depicted by the three dotted Gaussian-like curves in Fig. 1. The single-frequency field-magnitude (absolute value of H_z) distributions of features 1–3 are shown in Figs. 2(a)–2(c), respectively. Except feature 3, the coupling field distributions are localized indicating their LSP natures. The evaluated outward power flows along the Ag/dielectric interface of features 1 and 2 are negligibly small, confirming that they are LSP features. Feature 3 shows a broad field distribution in the x-y plane, indicating its grating-assisted SPP characteristics. It is noted that the weak emission of this SP feature (see Fig. 1) does not guarantee its effective SP energy storage. Other loss mechanisms, including SPP outward propagation along the interface and metal dissipation, may rapidly decrease SP energy. The locations labeled as A_{1-3}, B_{1-3}, C_3, and D_3 in Figs. 2(a)–2(c) are assigned as the observation points of the time-resolved study. Points A_{1-3} are located at the Ag/dielectric interface right above the dipole. Points A_3-D_3 are separated successively by one grating period.

Figure 3 shows the time-resolved intensity profiles of feature 1 (LSP) at the two observation points. Here, the source profile is also shown and labeled as S for reference. The intensity profiles at those observation points are normalized to the peak level at point A_1, which is normalized to the source peak level. The intensity profiles in a linear scale and normalized by the individual peak levels are shown in the insert. The response delay times from the source peak and the profile decay times are shown in Table I. The delay times at A_1 (5.39 fs) and B_1 (5.74 fs) represent the characteristic time constant for building the coupling system of feature 1. The fitted decay times of those profiles show the similar decay slopes, indicating that after the coupling system is built, the system releases energy with an effective decay time of $\sim 7-8$ fs.

Figure 4 shows the time-resolved intensity profiles of feature 2 (LSP) at the two observation points. Although the peak at A_2 can appear in a short time (2.92 fs), it takes ~ 7 fs for building the complete field distribution of the coupling system. The relatively shorter decay times in comparison to

TABLE I. Time-resolved signal parameters of the three SP-dipole coupling systems.

	Observation point	$A_{1,2,3}$	$B_{1,2,3}$	C_3	D_3
Feature 1	Delay time (fs)	5.39	5.74	···	···
(430 nm)	Decay time (fs)	6.92	7.55	···	···
Feature 2	Delay time (fs)	2.92	7.15	···	···
(520 nm)	Decay time (fs)	5.56	5.09	···	···
Feature 3	Delay time (fs)	1.12	9.33	14.32	19.26
(590 nm)	First decay time (fs)	4.11	13.11	13.09	14.32
	Second decay time (fs)	18.95	20.69	20.32	19.62

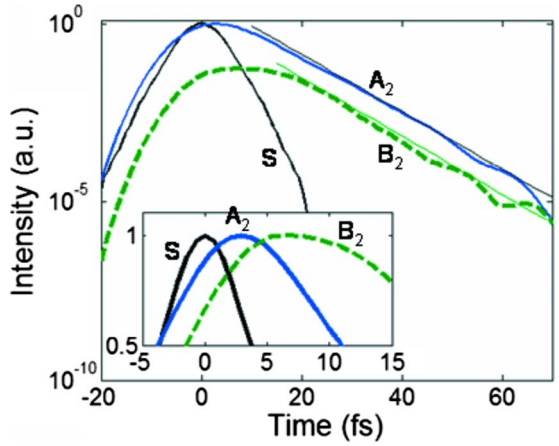

FIG. 4. (Color online) Similar to Fig. 3 except for feature 2.

feature 1 of ~5 fs at both observation points of this LSP feature are attributed to the more effective emission of this coupling system because the dissipation rates of the two LSP features, which are defined by the fixed metal damping factor γ, are supposed to be similar.

Figure 5 shows the time-resolved intensity profiles of feature 3 (grating-assisted SPP) at the four observation points. Here, effective coupling leads to a short buildup time at A_3 (1.12 fs). At B_3-D_3, energy is received mainly through SP outward propagation from A_3. Therefore, the peaks at C_3 and D_3 appear at about 5 and 10 fs later than that at B_3. We have used the plane-wave-assisted BIEM[17] to plot the dispersion curve of the concerned SPP. From the dispersion curve of feature 3, we can evaluate the group velocity of this SPP at 590 nm to give 1.99×10^7 m/s. The propagation of this SPP over a grating period (100 nm) with this group velocity accounts for the observed ~5 fs successive delays between B_3, C_3, and D_3. The longer delay at B_3 is due to the required period for building the local coupling. In Fig. 5, two decay

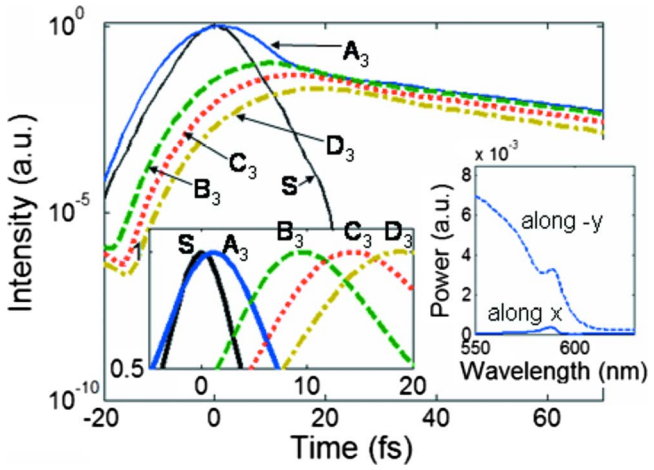

FIG. 5. (Color online) Similar to Fig. 3 except for feature 3. In the inset at the lower-right corner, we compare the along-interface outward propagating power (along x) at $x=\pm500$ nm and the bottom emission power (along $-y$) at 590 nm in wavelength.

components can be seen in all the response profiles. The first-stage decay is attributed to the outward SPP propagation from A_3. This stage ends when the intensity at B_3 is about the same as that at A_3. At this moment, the counterpropagation through grating diffraction results in negligible energy transport from a grating element into the neighboring ones. In the inset at the lower-right corner of Fig. 5, we compare the along-interface outward propagating power (along x) at $x=\pm500$ nm and the emission power (along $-y$) at 590 nm to show the much weaker along-interface propagation. Therefore, the SP energy in this grating-assisted SPP feature is well confined. The long decay time of ~20 fs in the second decay stage implies that such a SP feature has the potential of implementing a SPASER system. On the other hand, the two LSP-coupling features are useful for enhancing the efficiency of a light-emitting device.

In summary, we have demonstrated the transient behaviors of the dipole couplings with three SP features. The significantly longer decay time (in the second decay stage) of the grating-assisted SPP feature implied its potential application to SPASER implementation, while the efficient emissions and hence the shorter decay times of the LSP-coupling features implied their effective applications to emission enhancement.

This research was supported by the National Science Council, The Republic of China, under Grant Nos. NSC 96-2120-M-002-008 and NSC 96-2221-E-002-188 and by the U.S. Air Force Scientific Research Office under Contract No. AOARD-07-4010.

[1] A. Neogi, C. W. Lee, H. O. Everitt, T. Kuroda, A. Tacheuchi, and E. Yablonovitch, Phys. Rev. B **66**, 153305 (2002).
[2] K. T. Shimizu, W. K. Woo, B. R. Fisher, H. J. Eisler, and M. G. Bawendi, Phys. Rev. Lett. **89**, 117401 (2002).
[3] Y. Ito, K. Matsuda, and Y. Kanemitsu, Phys. Rev. B **75**, 033309 (2007).
[4] M. A. Noginov, G. Zhu, M. Bahoura, C. E. Small, C. Davison, J. Adegoke, V. P. Drachev, P. Nyga, and V. M. Shalaev, Phys. Rev. B **74**, 184203 (2006).
[5] K. Okamoto, I. Niki, A. Shvartser, Y. Narukawa, T. Mukai, and A. Scherer, Nature Mater. **3**, 601 (2004).
[6] G. Sun, J. B. Khurgin, and R. A. Soref, Appl. Phys. Lett. **90**, 111107 (2007).
[7] J. B. Khurgin, G. Sun, and R. A. Soref, J. Opt. Soc. Am. B **24**, 1968 (2007).
[8] D. M. Yeh, C. F. Huang, C. Y. Chen, Y. C. Lu, and C. C. Yang, Appl. Phys. Lett. **91**, 171103 (2007).
[9] D. M. Yeh, C. F. Huang, C. Y. Chen, Y. C. Lu, and C. C. Yang, Nanotechnology **19**, 345201 (2008).
[10] D. J. Bergman and M. I. Stockman, Phys. Rev. Lett. **90**, 027402 (2003).
[11] J. Seidel, S. Grafström, and L. Eng, Phys. Rev. Lett. **94**, 177401 (2005).
[12] J. Y. Wang, Y. W. Kiang, and C. C. Yang, Appl. Phys. Lett. **91**, 233104 (2007).
[13] K. C. Shen, C. Y. Chen, C. F. Huang, J. Y. Wang, Y. C. Lu, Y. W. Kiang, C. C. Yang, and Y. J. Yang, Appl. Phys. Lett. **92**, 013108 (2008).
[14] W. H. Chuang, J. Y. Wang, C. C. Yang, and Y. W. Kiang, Appl. Phys. Lett. **92**, 133115 (2008).
[15] W. H. Chuang, J. Y. Wang, C. C. Yang, and Y. W. Kiang, IEEE Photonics Technol. Lett. **20**, 1339 (2008).
[16] Y. Gong and J. Vučković, Appl. Phys. Lett. **90**, 033113 (2007).
[17] J. Y. Wang, C. C. Yang, and Y. W. Kiang, Opt. Express **15**, 9048 (2007).
[18] F. Wooten, *Optical Properties of Solids* (Academic, New York, 1972).